On the experimental determination of concrete compressive and tensile strengths

CLAUDIA A. MOREL – ASSIST. PROF. – https://orcid.org/0009-0003-6889-4063 (cmorel@ing.unne.edu.ar) — **Universidad Nacional del Nordeste, Argentina**
IGNACIO ITURRIOZ – PROF. – https://orcid.org/0000-0002-4918-9698 ;
JORGE RIERA – PROF. EMÉRITO – https://orcid.org/0000-0002-4902-237X — **UFGRS**

RESUMO

FOR DESIGN PURPOSES, CONCRETE IS OFTEN MODELLED AS A LINEARLY ELASTIC, ISOTROPIC AND HOMOGENEOUS MATERIAL. DIN CODES INITIALLY USED CUBIC SAMPLES TO ASSESS UNIAXIAL COMPRESSIVE STRENGTH, BUT FRICTION EFFECTS ALONG THE LOADING PLATES LED TO THEIR REPLACEMENT BY CYLINDERS. EVIDENCE THAT STRENGTH VARIES WITH THE CASTING DIRECTION RAISED DOUBT ABOUT THE IMPLICIT ISOTROPY ASSUMPTION. MEASURING THE COMPRESSIVE STRENGTH IN VERTICAL AND HORIZONTAL DIRECTIONS REQUIRES, HOWEVER, PROPERLY SUPPORTED CUBIC SAMPLES. TO ADDRESS THE FRICTION PROBLEM, GREASE PERFORMED BETTER THAN OTHER ALTERNATIVES AND WAS CHOSEN FOR DISCRETE ELEMENT METHOD (DEM) SIMULATIONS OF EXPERIMENTAL RESULTS. GREASED CUBIC SPECIMENS LED TO NEARLY THE SAME COMPRESSIVE STRENGTH MEASUREMENTS AS FOUND FOR CYLINDERS OR PRISMS, AND DETERMINED ANISOTROPY DUE TO THE CASTING DIRECTION. DEM SIMULATIONS ALSO SUGGEST THAT CUBIC SAMPLES CAN REPLACE CONVENTIONAL SPLITTING TENSILE STRENGTH TESTS, PROVIDING TENSILE STRENGTH DATA IN BOTH DIRECTIONS.

PALAVRAS-CHAVE: COMPRESSIVE STRENGTH; TESTING, APPARATUS & METHODS; DISCRETE-ELEMENT MODELLING; CONSTITUTIVE RELATIONS.

1. INTRODUCTION

For engineering design, under low-stress conditions, concrete is generally modelled as a linearly elastic, isotropic and homogeneous material. However, compressive and tensile strengths are assessed through tests on samples subjected to a non-uniform stress field. Conventional tests apply loads using rigid steel plates, which induce shear stresses that restrict lateral deformations and generate a triaxial stress state near the contact surfaces. This effect has not been fully

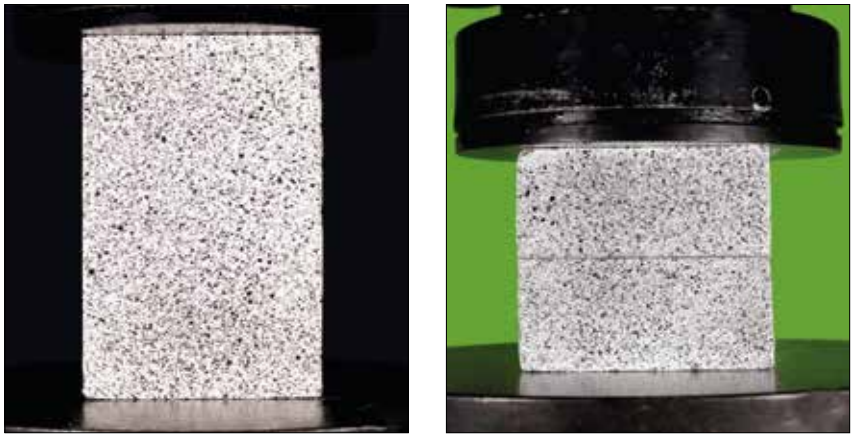

FIGURA 1
SPECIMEN GEOMETRIES: (A) PRISM, (B) CUBE

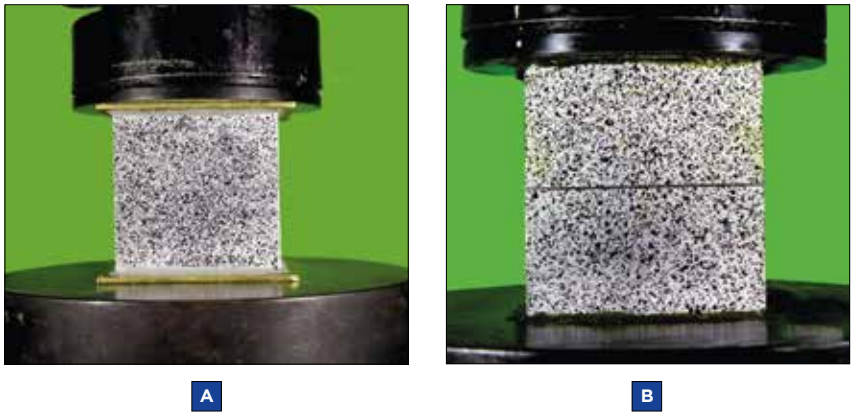

FIGURA 2
BOUNDARY CONDITIONS: (A) GLUED SHEETS, (B) GREASE

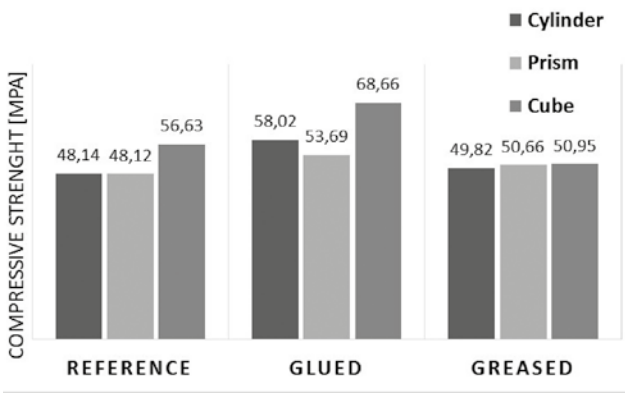

FIGURA 3
Compressive strength of C50 concrete according to geometry and boundary conditions

quantified, but Kotsovos(1983) and Wang et al(2024) used FEM models to analyze how friction between the plates and the sample affects the result. Experimental studies show that the compressive strength in vertically oriented cylindrical samples can be as much as 10% higher than in horizontally oriented samples.

Friction at the contact surfaces must be minimized when using cubic samples to measure strength in both orientations. Grease layers have proven more effective than other solutions in reducing friction. Bandeira *et al.* (2022) conducted tests under various boundary conditions on the loading plates, finding that grease performed best as an anti-friction solution. We select it, therefore, for numerical simulations using the discrete element method (DEM).

Riera *et al.* (2014) used DEM simulations to evaluate methods for determining the tensile strength of concrete, highlighting limitations due to material anisotropy. Previously, Rocco *et al.* (2001) had proposed using cubic samples to evaluate tensile strength in both directions, assessing concrete anisotropy, a scheme further examined in this paper.

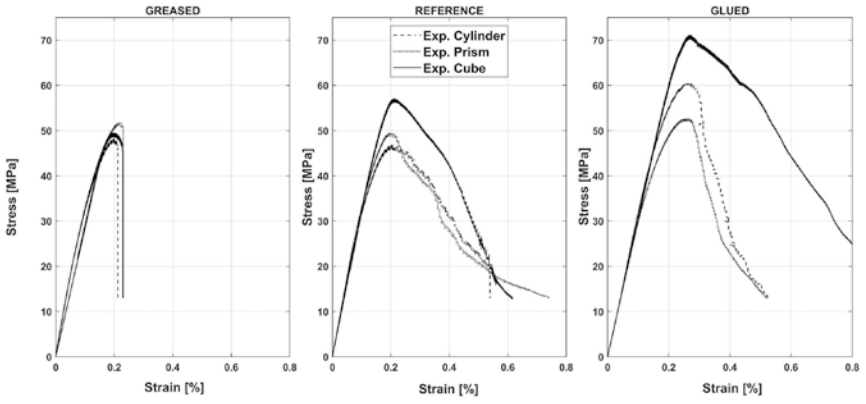

FIGURA 4
Plots of experimental mean stress–strain curves for C50 concrete

TABELA 1
The Composition of concrete mix C50 used in Bandeira *et al* (2022)

Feature	Cement [kg/m³]	Sand [kg/m³]	Aggregate [kg/m³]	Superplasticizer [kg/m³]	w/c
C50	445.59	794.44	1029.31	0.33	0.44

Wang *et al.* (2024) conducted similar simulations using FEM, reaching similar conclusions.

2. TEST DESCRIPTION

2.1 Experimental Assessments of Compressive Strength

The samples consisted of cylinders (20 cm height, 10 cm diameter), prisms (20 cm height, 10 cm square section), and cubes (10 cm edges). Concrete mixes with nominal strengths of 50 MPa (C50) and 30 MPa (C30) were used, previously studied by Kosteski *et al.* (2018); Bandeira *et al.* (2022); Vidal *et al.* (2020); Kosteski *et al.* (2019). A total of 104 specimens were cast, as shown in Figure 1. Bandeira *et al.* (2022) analyzed five boundary conditions, from which two were simulated: (a) the specimen ends in direct contact with steel plates, and (b) 3 mm metal sheets adhered to the faces, greased to reduce friction (Figure 2).

Four compression tests were performed for each geometry and boundary condition of the concrete mix. Figure 3 shows the average compressive strengths for the C50 concrete. Stress–strain curves for each case (Figure 4) reflect typical behaviour. Prisms and cylinders exhibited similar stress–strain behaviour in the reference and greased conditions. After peak load, specimens with greased interfaces rapidly lost compressive capacity. Table 1 shows, for reference, the C50 concrete composition as used by Bandeira *et al.* (2022).

Kumar *et al.* (2016) and Kotsovos (1983) noted that such behaviour aligns with brittle material responses. The observed toughness in tests with glued plates resulted from friction between the specimen and the machine, not from the material's intrinsic properties.

2.2 Splitting Tensile Test

The splitting tensile test, commonly referred to as the Brazilian Test, is a widely employed method for determining the tensile strength of concrete. Lobo Carneiro recognized the importance of using consistent sample size and geometry to determine compressive and tensile strength, though implicitly accepted the assumption

of isotropy. Rocco *et al.* (2001) examined the splitting tensile test standards, incorporating fracture mechanics concepts, noting that tensile strength values could vary by as much as 40% within the prescribed standards.

Rocco *et al.* (2001) also examined cylindrical and prismatic specimens, determining that the maximum tensile stress on the load plane depends on the width of the load-bearing strips and can be expressed as:

[1a] $$\sigma_{max} = \frac{2P}{\pi dh}\left(1-\beta^2\right)^{3/2}$$ for cylindrical specimens

[1b] $$\sigma_{max} = \frac{2P}{\pi dh}\left[\left(1-\beta^2\right)^{5/3} - 0.0115\right]$$ for prismatic specimens

Here, d and h denote the specimen's dimensions, P is the applied load, and β is the ratio of the load-bearing strip width to the specimen diameter or side length. These equations hold for β ≤ 0.20. For brittle, linear-elastic materials, failure is assumed to occur when the maximum tensile stress reaches a critical value, corresponding to the material's tensile strength f_{ct}. Thus, the failure criterion is:

[2a] $$f_{ct} = \frac{2P_u}{\pi dh}\left(1-\beta^2\right)^{3/2}$$ for cylindrical specimens

[2b] $$f_{ct} = \frac{2P_u}{\pi dh}\left[\left(1-\beta^2\right)^{5/3} - 0.0115\right]$$ for prismatic specimens

Where P_u is the maximum load recorded during the test. By definition, f_{ct} corresponds to a cylinder's theoretical splitting tensile strength when β = 0. It should be noted that small values of β may not meet these assumptions. The splitting tensile strength from the standard test is given by Equation (2) and, incorporating Equation (1), can be rewritten as:

[3a] $$f_{ctsp,c} = f_{ct}\left(1-\beta^2\right)^{-3/2}$$ for cylindrical specimens

[3b] $$f_{ctsp,q} = f_{ct}\left[\left(1-\beta^2\right)^{5/3} - 0.0115\right]^{-1}$$ for prismatic specimens

Where $f_{ctsp,c}$ and $f_{ctsp,q}$ represent the splitting tensile strengths of cylinders and prisms, respectively. The equations provide the tensile strength in the horizontal direction, which may differ significantly from the vertical tensile strength. Therefore, the degree of anisotropy remains undetermined.

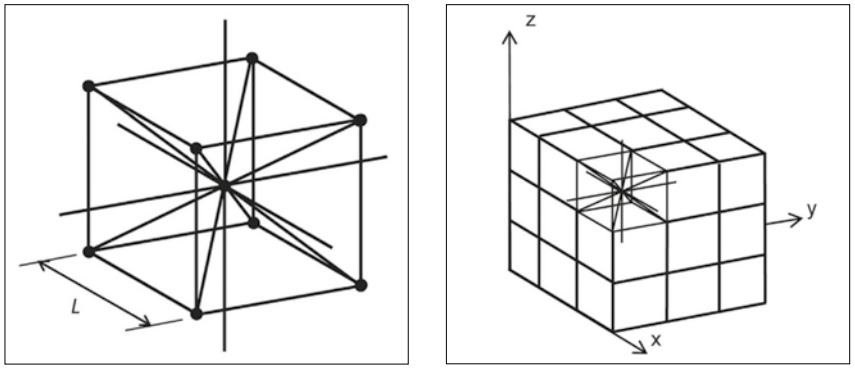

FIGURA 5
DEM MODELS: (A) BASIC CUBIC MODULE, (B) PRISM FORMED FROM MULTIPLE CUBIC MODULES

3. DISCRETE ELEMENT METHOD

The Discrete Element Method (DEM) represents a continuum using a periodic array of bars with masses concentrated at nodes. As shown in Figure 5, a basic cubic module consists of twenty bars and nine nodes, and each node has three degrees of freedom, enabling the determination of displacements in a global reference system.

Applying Newton's second law, the system of equations is obtained by writing, for each node:

[4] $$\boldsymbol{M\ddot{x}(t) + C\dot{x}(t) + F(t) - P(t) = 0}$$

$\ddot{\boldsymbol{x}}(t)$ and $\dot{\boldsymbol{x}}(t)$ are the nodal accelerations and velocities, and M and C are the mass and damping matrices, respectively. As these matrices are diagonal, the equa-

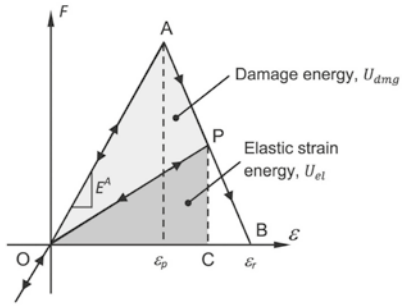

FIGURA 6
BILINEAR CONSTITUTIVE MODEL

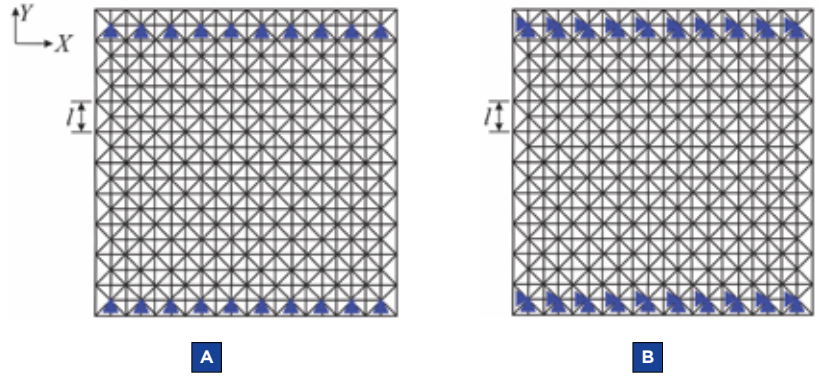

FIGURA 7
RESTRICTIONS ON NODE MOBILITY. (A) CONSTRAINED ON THE Y AXIS ALONE, (B) CONSTRAINED ON BOTH THE X AND Y AXES

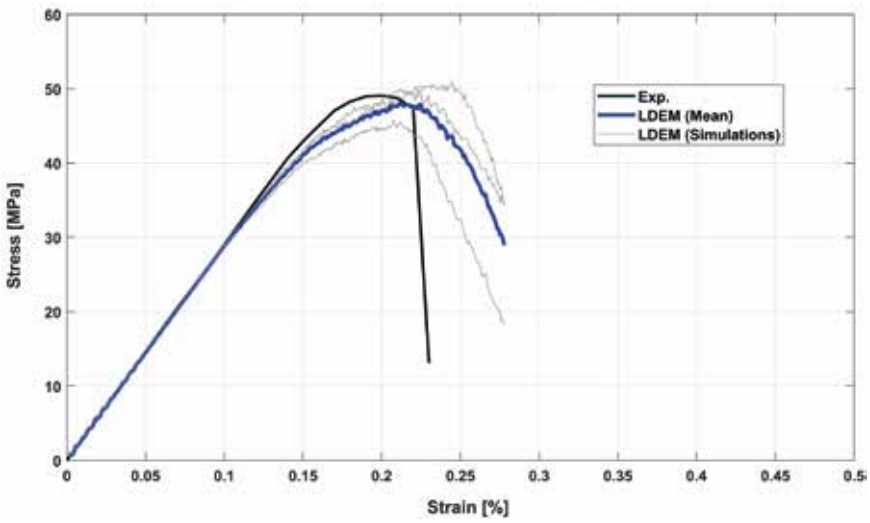

FIGURA 8
Mean experimental and simulated curves for the cube with greased boundaries jointly with three DEM simulations

TABELA 2
Parameters adopted in DEM simulations for compression tests

Length of cubic element L_c	0.01m
DEM modules in x, y, z directions (cube)	11, 11, 11
DEM modules in x, y, z directions (prism)	11, 21, 11
Poisson ratio v	0.25
Specific mass [ρ]	2400 kg/m³
Young's modulus [E]	32 GPa
μG_f	150 N/m
CVG_f	100%
$\mu(\varepsilon_p)$	0.0004

tions are decoupled, allowing time-domain integration using an explicit finite difference scheme. This approach simplifies handling large displacements as the nodal positions are updated at each time step.

Rocha *et al.* (1991) and Kosteski *et al.* (2011) developed nonlinear constitutive models for quasi-brittle materials, as illustrated in Figure 6. The area under the force–strain curve (the area of triangle OAB in Figure 6) represents the energy required to fracture the element. Failure occurs when the dissipated energy equals the fracture energy.

The elements remain linearly elastic in compression, with failure induced indirectly through tensile stresses. The energy dissipated by the fracture of a DEM module is given by:

$$[5] \quad \Gamma_{LDEM} = G_f c_A \left[(4)(0.25) + 1 + 4\left(\frac{2}{\sqrt{3}}\delta\right)\right] L_c^2$$

Where G_f = specific fracture energy (N/m);
C_A = scale parameter;
δ = density of the material (kg/m³) and;
L_c = length of longitudinal elements in the cubic DEM arrangement (m).

The critical strain can be obtained from the following relationship:

$$[6] \quad \varepsilon_p = \sqrt{\frac{G_f}{d_{eq} E}}$$

Where denotes a material parameter (m).

Furthermore, Carpinteri's brittleness number is adapted to DEM as a measure of ductility based on the characteristic length of the material R.

$$[7] \quad s = \sqrt{\frac{d_{eq}}{R}}$$

In DEM models, constitutive laws are influenced by both material properties and the discretization level. Mesh perturbations do not significantly alter the stiffness of elements, improving model performance under compressive loads. Additionally, DEM has been effectively applied to study size effects in quasi-brittle materials, a phenomenon previously explored in various studies such as Kosteski *et al.* (2011).

4. COMPUTATIONAL MODELS

Cubic samples with 10 cm sides were used in this study. Two boundary conditions, shown in Figure 2, were simulated:

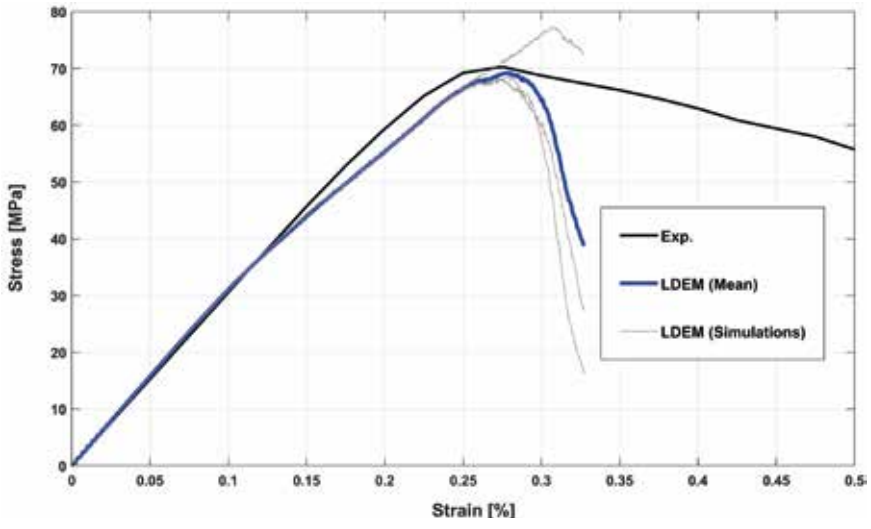

FIGURA 9
Mean experimental and simulated curves for the cube with glued plates jointly with three DEM simulations

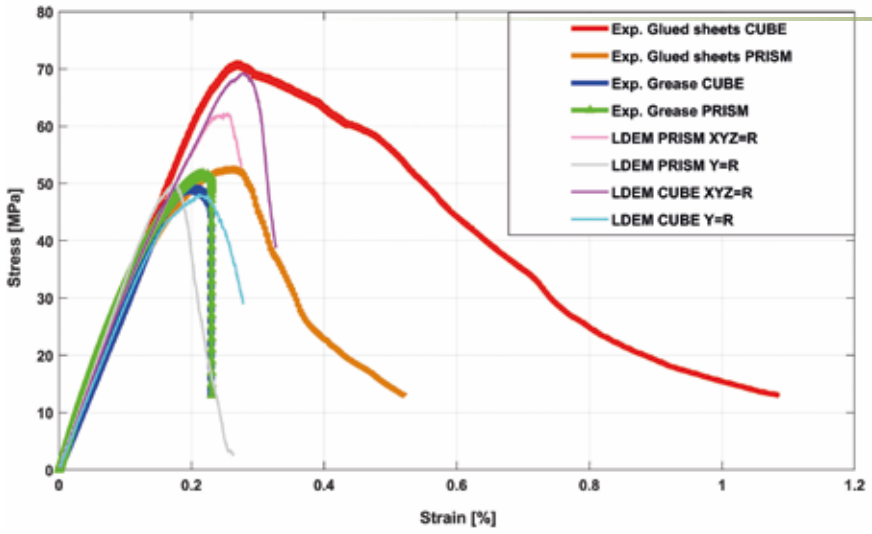

FIGURA 10
Experimental mean stress vs mean strain curves for prisms with greased and glued plates, jointly with DEM predictions for cubes and prisms with and without lateral restriction at the boundaries

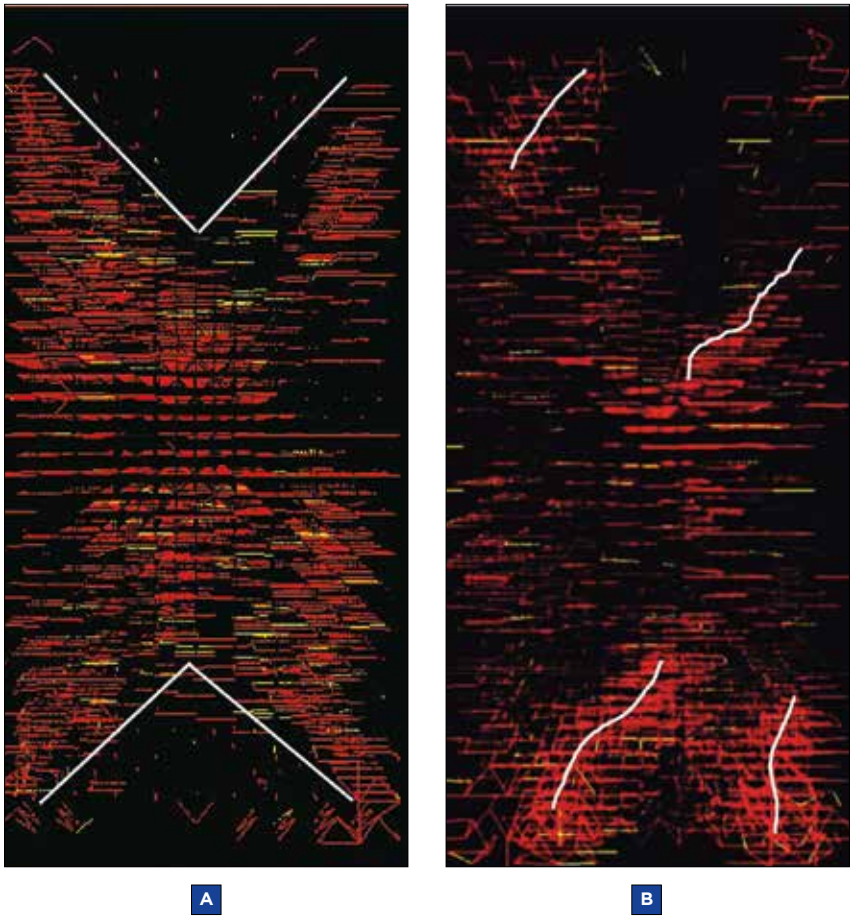

FIGURA 11
Typical rupture configuration for prismatic samples under compression is (a) horizontal displacements restrained at upper and lower faces and (b) frictionless boundaries

(a) glued upper and lower plates and (b) grease layers to reduce friction. Uncertainties in these boundary conditions were considered negligible.

For the glued plates, prescribed vertical displacements were applied at the upper end, simulating the action of the upper loading plate on a specimen under compression. In contrast, horizontal displacements of the nodes shown are zero. Nodes at the lower surface are considered fixed. In the grease-layer setup, a thin viscous fluid was assumed between the plates and the cube surfaces, resulting in vertical displacements normal to the surface. In this case, nodes could move horizontally.

Figure 7(a) represents the restrictions for tests with grease layers, while Figure 7(b) corresponds to tests with glued plates. Table 2 summarizes the parameters adopted for the DEM simulations in compression tests.

5. DEM PREDICTIONS OF COMPRESSION TEST RESULTS

This section compares the average vertical stress and strain from the experiments by Bandeira *et al.* (2022) with DEM simulation predictions. Figure 8 shows the experimental curve for the cube with greased boundaries, along with three DEM simulations and their average. Similarly, Figure 9 presents the experimental curve for the cube with glued plates, with corresponding DEM simulations. Both figures highlight the effect of boundary

TABELA 3
Parameters adopted in DEM simulations for indirect tensile testing

Length of cubic element L_c	0.01 m
DEM modules in x, y, z directions (cube)	16, 16, 16
Poisson ratio v	0.25
Specific mass [ρ]	2400 kg/m^3
Young's modulus [E]	33.0 GPa
μG_f	150 N/m
CVG_f	50%
$\mu(\varepsilon_p)$	0.0002

conditions on the results. Finally, Figure 10 displays mean stress-strain curves for prisms with reference, greased, and glued plates, along with DEM predictions for cubes with greased boundaries. The numerical DEM predictions align closely with the experimental measurements of both the strength and the average strain, particularly at the peak stress value for cubes, prisms, and under all boundary conditions. The unconfined uniaxial compressive strength is primarily determined by the prisms (or cylinders) and by the cubes with grease.

The strength observed is influenced by boundary conditions, meaning it cannot be considered a material property. The numerical simulations, which assume consistent material properties, confirm this. However, the boundary conditions in the simulations only approximate those in the tests for mean strains below the peak strain. Figure 10 highlights differences in failure stress between numerical and experimental tests when lateral displacement is restricted. In contrast, when lateral displacements are unrestricted, the failure stress for prisms and cubes aligns, suggesting that it can be treated as a material property under these conditions.

Uncertainties increase significantly during the softening phase. For example, assuming that all boundary nodes on the upper and lower surfaces remain coplanar throughout the test becomes questionable once large cracks form. In frictionless tests, cracks develop nearly perpendicular to the load direction, a phenomenon more evident in the cubes (Figure 12) than in the prisms (Figure 11). Material variability influences fracture locations, resulting in unique patterns for each test (see also Bandeira *et al.* (2022). Cubic and prismatic models with glued plates show pyramidal patterns at both ends, as illustrated in Figures 11 and 12. The damage patterns are visualized using Paraview.

The strength with glued plates – where horizontal displacements are restricted – is about 40% higher than in frictionless cubes, closely matching the

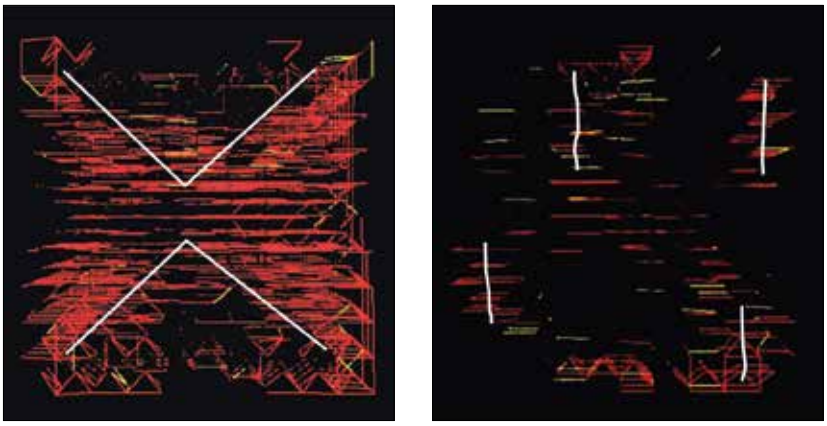

FIGURA 12
Typical rupture configuration for cubic samples under compression is (a) horizontal displacements restrained at both upper and lower faces and (b) frictionless boundaries

results by Bandeira *et al.* (2022). In case (a), fractures form at 45° at both ends, and the concrete fails by indirect tension, creating six pyramids. In some cases, sliding with friction follows, determining the softening branch. Post-peak curves differ between tests and cannot be considered a material property.

6. DEM PREDICTIONS OF INDIRECT TENSION TEST RESULTS

Cubic models with 15 cm side lengths were simulated in indirect tensile tests. Figure 13 illustrates the boundary conditions. Vertical displacements are specified at the upper face, simulating the effect of the upper bearing strip under load P in a splitting test. The indicated nodes remain unrestricted in the horizontal plane.

Min *et al.* (2014) report the experimental results used for comparison. Table 3 lists the values used in the DEM simulations. Figure 14 shows the

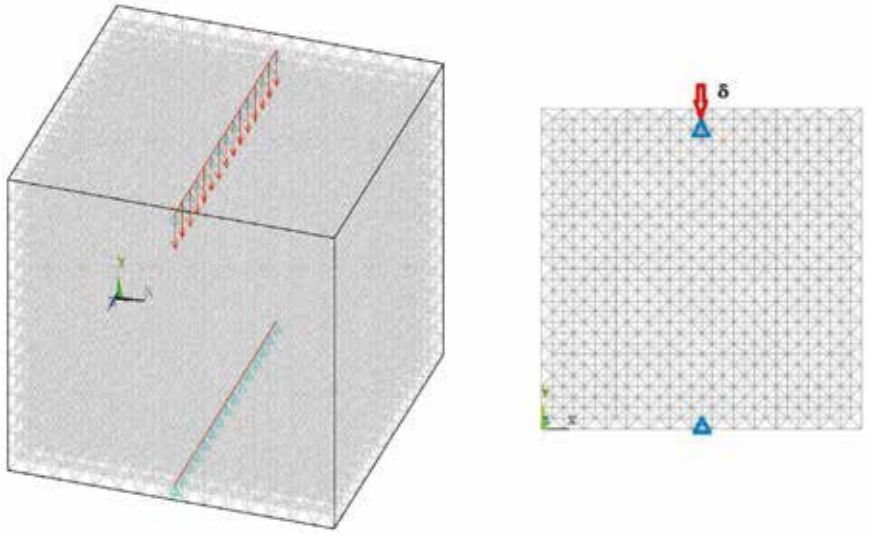

FIGURA 13
Boundary conditions for indirect tensile test simulation

force–strain curve of a cube with DEM predictions for the indirect tensile test. In the study by Min *et al.* (2014), the maximum load values varied between 121 kN and 124.7 kN, providing crucial insights into the mechanical behaviour under consideration.

Numerical DEM results closely reproduce experimental values of both peaks of the force and indirect tensile strength of the cube (Min *et al.*, 2014). Damage patterns, visualized using Paraview, are shown in Figure 15. The model breaks by indirect traction, resulting in a neat failure plane in the middle of the cube. The horizontal tensile stress associated with the splitting test may be determined using expression 2b, in which P_u = 149 kN, d = h = 0.15m, and b = 1/15, yielding a tensile stress f_{ct} = 4.13 Mpa, a value compatible with the tensile stress specified in the input data, that is $f_{ct} = \mu(\varepsilon p)xE$ = 6.6 MPa.

7. CONCLUSIONS

Numerical simulations confirmed that tests on cubic samples with frictionless upper and lower supports provide comparable measures of the unconfined compressive strength of concrete to those obtained from standard tests on cylinders or prisms. Among the various methods proposed in the technical literature to minimize friction, only grease consistently satisfies the zero-friction condition in the simulations.

An advantage of using cubic samples is the ability to measure concrete compressive strength *in orientations normal to the casting direction* (horizontal directions). This is particularly relevant because, in standard splitting tensile tests, the tensile strength measured corresponds to a horizontal direction, which is often assumed – despite experimental evidence – to be identical in all orientations. Further investigation into the differences between concrete strengths in vertical and horizontal directions requires frictionless tests *on cubic samples*.

A key finding of this study is that the post-peak behavior observed in the numerical simulations depends primarily on the testing conditions rather than on material properties. This observation highlights the limitations of DEM simulations in their current formulation for capturing the softening branch, as large fractures may close and sliding with friction along fracture surfaces introduces uncertainty. The accuracy of the simulations is highly dependent on the testing conditions and any change in these conditions could significantly alter the results.

Additionally, DEM simulations of the splitting tensile test performed on cubes show promising results, warranting further experimental validation to confirm their applicability and accuracy.

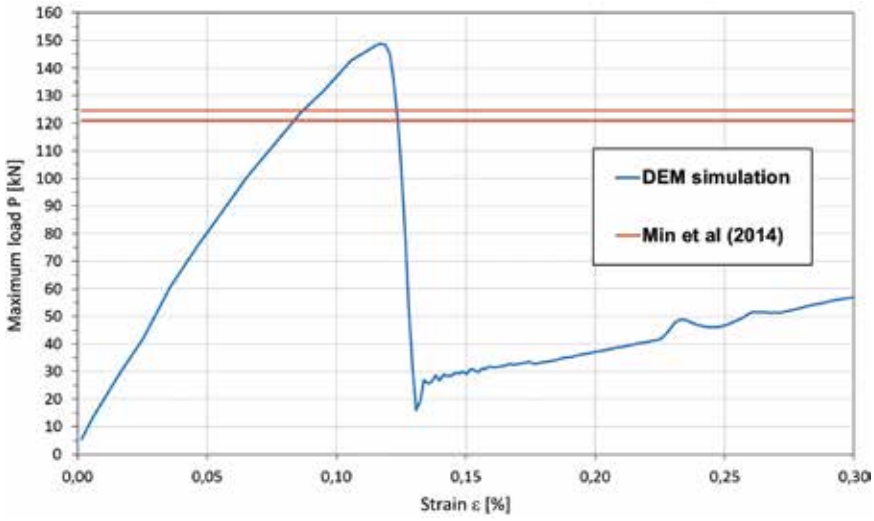

FIGURA 14
DEM PREDICTION VS. LOAD IN INDIRECT TENSILE TEST

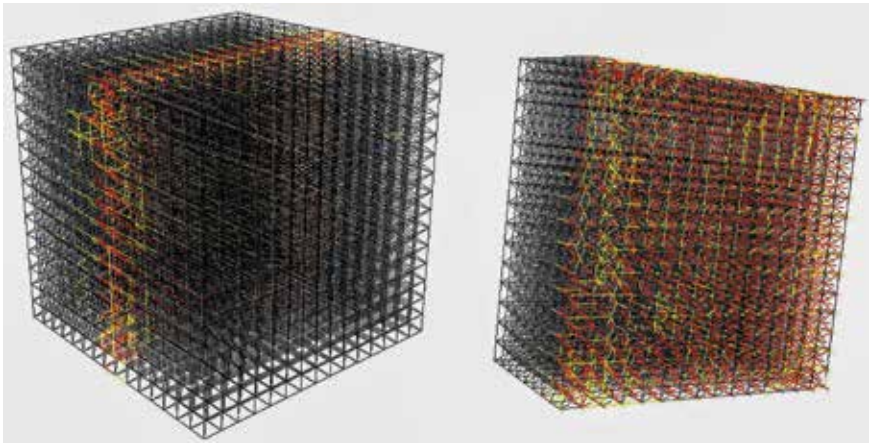

FIGURA 15
TYPICAL RUPTURE CONFIGURATION FOR CUBIC SAMPLE UNDER INDIRECT TENSILE TEST. AXONOMETRIC VIEW AND CROSS-SECTION. THE BROKEN BARS ARE INDICATED IN RED, AND THE DAMAGED BARS IN YELLOW

ACKNOWLEDGEMENTS

This project was supported by CNPq, CAPES, and FAPERGS (Brazil). The authors thank Dr Juan Manuel Vallejos, Eng Julio César Molina and MSc Ricardo Barrios D'Ambra for their assistance in editing some of the figures in this paper.

▶ REFERÊNCIAS BIBLIOGRÁFICAS

[1] BANDEIRA, M. V. V.; LA TORRE, K. R.; KOSTESKI, L. E.; MARANGON, E.; RIERA, J. D. Influence of contact friction in compression tests of concrete samples. *Construction and Building Materials*, vol. 317, 2022, 125811.

[2] KOTSOVOS, M. D. Effect of testing techniques on the post-ultimate behaviour of concrete in compression. *Matériaux Constr.*, 1983.

[3] KOSTESKI, L.; ITURRIOZ, I.; GALIANO, B. R.; CISILINO, A. P. The truss-like discrete element method in fracture and damage mechanics. *Engineering Computations*, vol. 28, no. 6, 2011, 765-787.

[4] KOSTESKI, L. E.; MARANGON, E.; RIERA, J. D.; KECHE DOS SANTOS, F. J.; BANDEIRA, M. V. V. Assessment of concrete anisotropy in relation to the direction of casting. *Rev. Sul-americana Eng. Estrutural*, 2018.

[5] KOSTESKI, L. E.; MARANGON, E.; RIERA, J. D. Assessment of concrete anisotropy by means of compression and indirect tensile tests. *Rev. IBRACON Estruturas e Mater.*, 2019.

[6] KUMAR, S.; MUKHOPADHYA, T.; WASEEM, S. A.; SINGH, B.; IQBAL, M. A. Effect of Platen Restraint on Stress-Strain Behaviour of Concrete Under Uniaxial Compression: a Comparative Study. *Strength Mater*, 2016.

[7] MIN, F.; ZHANHU, Y.; TENG, J. Experimental and Numerical Study on Tensile Strength of Concrete under Different Strain Rates. *The Scientific World Journal*, vol. 2014, Article ID 173531, 2014, 11 páginas.

[8] RIERA, J. D.; MIGUEL, L. F. F.; ITURRIOZ, I. Assessment of Brazilian Tensile Test by means of the truss-like Discrete Element Method (DEM) with imperfect mesh. *Engineering Structures*, vol. 81, 2014, 10-21.

[9] ROCHA, M. M.; RIERA, J. D.; DE KRUTZIK, N. J. Extension of a Model that Aptly Describes Fracture of Plain Concrete to the Impact Analysis of Reinforced Concrete. In: *Int. Conf. and Structural Mechanics in Reactor Technology, SMIRT 11*, Trans. Vol. J. Tokyo, Japão, 1991.

[10] ROCCO, C.; GUINEA, G. V.; PLANAS, J.; ELICES, M. Review of the splitting-test standards from a fracture mechanics point of view. *Cement and Concrete Research*, vol. 31, 2001, 73-82.

[11] VIDAL, D. M. C.; BANDEIRA, V. V. M.; LA TORRE, R. K.; KOSTESKI, L. E.; MARANGON, E. Numerical and experimental evaluation of the anisotropic behaviour and boundary condition of a structural concrete. *Constr. Build. Mater.*, vol. 260, 2020.

[12] WANG, J.; YU, X.; FU, Y.; ZHOU, G. A 3-D meso-scale model and numerical uniaxial compression tests on concrete with consideration of the friction effect. *Materials*, vol. 17, no. 5, 1024, 2024.